THE PRE-DEPRESSION INVESTIGATION OF CLOUD-SYSTEMS IN THE TROPICS (PREDICT) EXPERIMENT

Scientific Basis, New Analysis Tools, and Some First Results

BY MICHAEL T. MONTGOMERY, CHRISTOPHER DAVIS, TIMOTHY DUNKERTON, ZHUO WANG, CHRISTOPHER VELDEN, RYAN TORN, SHARANYA J. MAJUMDAR, FUQING ZHANG, ROGER K. SMITH, LANCE BOSART, MICHAEL M. BELL, JENNIFER S. HAASE, ANDREW HEYMSFIELD, JORGEN JENSEN, TERESA CAMPOS, AND MARK A. BOOTHE

A field study involving 25 flights into Atlantic tropical disturbances tested the principal hypotheses of a new model of tropical cyclogenesis, known as the marsupial paradigm.

A longstanding challenge for hurricane forecasters, theoreticians, and numerical weather forecast systems is to distinguish tropical waves that will develop into hurricanes from tropical waves that will not. While tropical easterly waves occur frequently over the Atlantic and east Pacific, only a small fraction of these waves (~20%; e.g., Frank 1970) evolve into tropical storms when averaged over the hurricane season. The problem was insightfully summarized by Gray (1998): "It seems unlikely that the formation of tropical cyclones will be adequately understood until we more thoroughly document the physical differences between those systems which develop into tropical cyclones from those prominent tropical disturbances which have a favorable climatological and synoptic environment, look very much like they will develop but still do not."

The formation of tropical cyclones (TCs) is one of the remaining mysteries of the atmosphere (Emanuel 2005). As for why it remains unsolved, after decades of research, it is unfortunately true that in situ observations are lacking over remote tropical oceans. Recent years have seen several field campaigns aimed at understanding the science of tropical cyclone formation. These include the National Aeronautics and Space Administration (NASA) Tropical Cloud Systems and Processes (TCSP) experiment in 2005 (Halverson et al. 2007), the NASA African Multi-Disciplinary Monsoon Analyses (NAMMA) project in 2006 (Zipser et al. 2009), and the Tropical Cyclone Structure experiment in 2008 (TCS-08; Elsberry and Harr 2008). Adding the results of earlier efforts such as the Tropical Experiment in Mexico (TEXMEX; Bister and Emanuel 1997; Raymond et al. 1998) and even serendipitous observations of the early intensification of Hurricane Ophelia in the Hurricane Rainband and Intensity Change Experiment (RAINEX; Houze et al. 2006), and occasional observations from reconnaissance aircraft (Reasor et al. 2005), we have a collection of studies that have sampled pieces of a large and complex scientific puzzle. However, with the exception of the TCS08 experiment, the greatest shortcoming of previous campaigns has been the limited in situ observational sampling, both in space and in time. It has been difficult to piece together snapshots of tropical disturbances taken at different times. "Genesis" (defined here as

the formation of a tropical depression[1] at subsynoptic scales) often occurs between sampling times, or after disturbances move out of range.

There are very few in situ observations of both precursors to genesis and the ensuing tropical cyclone formation process. The paucity of observations is aggravated by a lack of a priori knowledge of where to sample a candidate disturbance. For a typical African/Atlantic easterly wave, the trough axis extends meridionally over a thousand kilometers or more. The dimension of a tropical storm in this sector is much smaller, a few hundred kilometers. Convective clouds and cloud systems are smaller still. Tropical cyclone formation is intrinsically a multiscale process (e.g., Gray 1998). The fate of a tropical easterly wave depends on the large-scale environment in which it is embedded, the wave's synoptic structure (e.g., low-level vorticity and middle-level moisture), and convective-scale processes associated with the wave's evolution. The large-scale necessary conditions for tropical cyclone formation have been known for over four decades (e.g., Gray 1968; DeMaria et al. 2001): nonzero cyclonic vorticity in the lower troposphere, sufficiently warm sea surface temperatures (≥26°C), a moist middle troposphere, and at most a moderate vertical shear between upper and lower troposphere (no larger than approximately 12 m s^{-1}). Some observational studies have suggested also that the upper-level environmental conditions over a developing low-level disturbance may play an important modulating role (Dvorak 1975; Sadler 1976; McBride and Zehr 1981). Yet, all of these conditions in conjunction are well known to be insufficient.

In late summer 2010 a trio of field campaigns was conducted by NASA, the National Oceanic and Atmospheric Administration (NOAA), and the National Science Foundation (NSF) to investigate tropical cyclogenesis in the Caribbean and west Atlantic and the subsequent intensification of named storms in these regions. While two of the campaigns[2] included intensification in their portfolio of objectives, the Pre-Depression Investigation of Cloud-Systems in the Tropics (PREDICT) campaign was designed exclusively to study genesis. Priority was given to developing storms prior to their classification as tropical depressions even when mature storms were present nearby. The primary measurement platform of PREDICT was the NSF–National Center for Atmospheric Research (NCAR) Gulfstream V (GV), equipped with dropsondes and onboard sensors for meteorological variables and ice microphysics (see Table 1). The range and speed of the GV, and the high altitude (~12–13 km) from which it could release dropsondes, were exploited to sample storm formation from Central America to the mid-Atlantic

[1] The glossary on NOAA's Hurricane Research Division's website uses "tropical cyclone as the generic term for a nonfrontal synoptic-scale low-pressure system over tropical or sub-tropical waters with organized convection (i.e. thunderstorm activity) and a definite cyclonic surface wind circulation." Notably, this definition does not invoke any wind threshold. The same glossary defines a "tropical depression" as a tropical cyclone with maximum sustained surface winds of less than 17 m s^{-1} (34 kt, 39 mph, and, in the Atlantic and eastern Pacific basins, a "tropical storm" as a tropical cyclone with surface winds between 17 and 33 m s^{-1}. In this study we will define genesis as the formation of a tropical depression and we impose no formal threshold on wind speed.

[2] The Genesis and Rapid Intensification Processes (GRIP) project of the National Aeronautics and Space Administration and the Intensify Forecasting Experiment (IFEX) of the National Oceanic and Atmospheric Administration.

AFFILIATIONS: Montgomery, Bell, and Boothe—Department of Meteorology, Naval Postgraduate School, Monterey, California; Dunkerton— Northwest Research Associates, Bellevue, Washington; Davis, Heymsfield, Jensen, and Campos—National Center for Atmospheric Research, Boulder, Colorado; Wang—Department of Atmospheric Sciences, University of Illinois at Urbana—Champaign, Urbana, Illinois; Velden—University of Wisconsin/CIMSS, Madison, Wisconsin; Torn and Bosart—Department of Atmospheric and Environmental Sciences, University at Albany, State University of New York, Albany, New York; Majumdar—Rosenstiel School of Marine and Atmospheric Science, University of Miami, Miami, Florida; Zhang—Department of Meteorology, Pennsylvania State University, University Park, Pennsylvania; Smith—Meteorological Institute, Ludwig-Maximilians University, Munich, Germany; Haase—Department of Earth and Atmospheric Sciences, Purdue University, West Lafayette, Indiana
ADDITIONAL AFFILIATIONS: Montgomery and Bell—NOAA's Hurricane Research Division, Miami, Florida; Dunkerton— Naval Postgraduate School, Monterey, California
CORRESPONDING AUTHOR: Michael Montgomery, Naval Postgraduate School Department of Meteorology, 1 University Circle, Monterey, CA 93943
E-mail: mtmontgo@nps.edu

The abstract for this article can be found in this issue, following the table of contents.
DOI:10.1175/BAMS-D-11-00046.1

In final form 22 July 2011

(roughly 40°W) operating out of St. Croix in the U.S. Virgin Islands (see Fig. 1).

The purpose of this article is to present an overview of the scientific basis for PREDICT, a summary of the scientific products used during the experiment, and some noteworthy first results that have emerged since the completion of the field phase on 30 September 2010. An outline of the remaining paper is as follows. A summary of the scientific basis of the experiment and practical impacts is presented in section 2. Section 3 presents a glimpse of the daily weather briefings and research tools employed to assess candidate tropical disturbances for possible flight operations. Section 4 presents a summary of all of the disturbances flown during the field program and provides some first clues as to the development versus nondevelopment issue. Section 5 provides our conclusions about the field phase of this work and sketches a path forward.

Table 1. Instrumentation payload on the NSF/NCAR GV research aircraft.

State parameters	Pressure	
	Temperature (3x)	
	Dewpoint	Buck Research
	Water vapor density	VCSEL and CARI TDL
Position	Honeywell IRS	
	Novatel GPS	
3-D wind	Dynamic pressure (2x)	Honeywell
	Attack/sideslip	Honeywell in radome
	Attack/sideslip	Honeywell in gust pod
Microphysics	Icing rate	Rosemount
	Liquid water content	DMT King probe
	Cloud droplets/ice	DMT CDP probe
	Ice particles	PMS/DMT 2D-C
	Ice particles	SPEC 3V-CPI
	Condensation nuclei	TSI water CN
	Aerosol particles	DMT UHSAS
	Aerosol particles	CVI
Remote sensing	Temperature profile	JPL Microwave Temperature Profiler
	Water vapor profile	Purdue GISMOS
	True air speed	EOL LAMS
Dropsondes	Pressure, temperature, dewpoint, wind	EOL/Vaisala GPS sonde

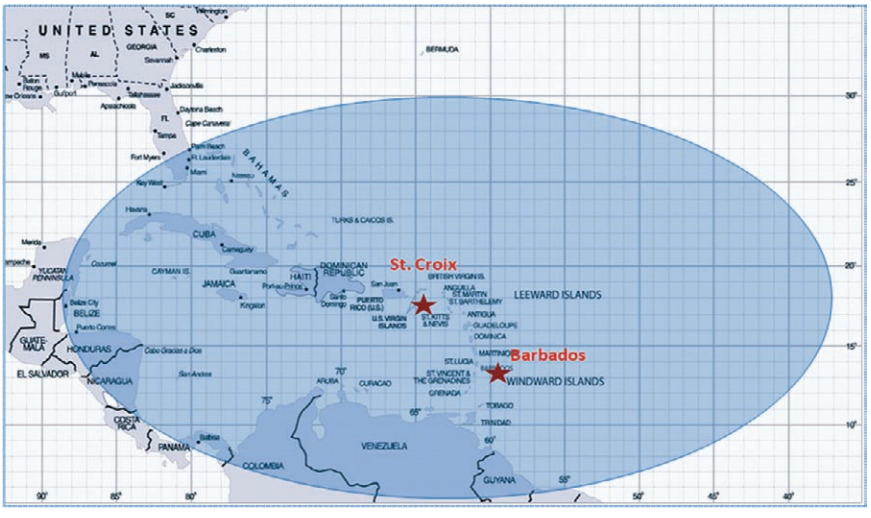

Fig. 1. PREDICT domain. The primary base of operations was St. Croix, VI, with an alternate of Barbados.

SCIENTIFIC BASIS AND PRACTICAL IMPACTS. In the experiment's conception it was recognized that tropical cyclogenesis is inherently a multiscale process (Gray 1998) as noted above. What the experiment needed was an overarching framework within which the roles of different scales could be evaluated to determine their relative importance in genesis over the western Atlantic, with presumably strong implications for genesis in other basins. The guiding philosophy for investigation was the following:

Tropical depression formation is greatly favored in the critical-layer region of the synoptic-scale predepression wave or subtropical disturbance.

This idea is the underlying tenet of a new model for cyclogenesis in tropical waves developed by Dunkerton et al. (2009, hereafter DMW09), expressed in three hypotheses (H1, H2, and H3). In basic fluid dynamical terms, the *cat's eye* recirculation region within the *critical layer* of the parent wave is a region of cyclonic rotation and weak straining deformation (H1). This region provides a set of approximately closed material contours. Inside the cat's eye circulation, air tends to be repeatedly moistened by cumulus convection, protected to some degree from lateral intrusion of dry air and deformation by horizontal or vertical shear, and (thanks to its location near the critical level) able to keep pace with the parent wave until the dominant vortex has strengthened into a self-maintaining entity (H2). During this time the parent wave is maintained and possibly enhanced by diabatically amplified eddies within the wave (protovortices on the mesoscale), a process favored in regions of small intrinsic phase speed (H3). The combination of the associated genesis sequence and the overarching framework for describing how such hybrid wave–vortex structures become tropical depressions/storms is likened to the development of a marsupial infant in its mother's pouch, and for this reason has been charmingly dubbed the "marsupial paradigm." This model is often referred to simply as the "pouch theory."

The new model finds strong support in the four-season observational survey of the Atlantic and eastern Pacific sectors carried out by DMW09, two recent case studies in the western Pacific sector during the Tropical Cyclone Structure 2008 (TCS08) field experiment (Montgomery et al. 2010a; Raymond and López-Carillo 2011), the post-analysis of the 2009 PREDICT Dry Run (Wang et al. 2011), and real-case and idealized high-resolution numerical model simulations (Wang et al. 2010a,b; Montgomery et al. 2010b; Fang and Zhang 2010, 2011). Together, these studies point to the pouch center as the preferred location (or "sweet spot") for cyclogenesis, serving as a "focal point" for an upscale vorticity aggregation process while the wave pouch and proto-vortex move together. As an outgrowth of these basic investigations, a Galilean invariant real-time wave tracking algorithm was developed to predict the possible loci of tropical cyclogenesis within the trough region of westward-propagating disturbances (Wang et al. 2009).

Of significance to forecasters is that the wave pouch provides a favorable local environment for the formation and intensification of the tropical cyclone protovortex. An immediate consequence of the new model is that the pouch provides a more precise, dynamically relevant target for continuous monitoring that is distinct from the chaotic moist convective activity that is scattered throughout the parent wave's trough. While deep convection outside, or along the edge, of the pouch can be equally vigorous, its longer-term impacts are subject to strain/shear deformation, inimical to development.

To distinguish developing from nondeveloping waves in the field campaign, and in future studies, we believe that a more complete understanding of the kinematic, dynamic, and thermodynamic aspects of the wave's pouch is essential. An improved understanding of the pouch structure has practical benefits as well. Since the subsynoptic-scale wave pouch can be resolved to some extent by coarse-resolution global model analyses and operational data, and predicted several days in advance, a proper diagnosis of the wave pouch can provide useful information to operational forecasters (Wang et al. 2009).

In summary, the main aim of the PREDICT experiment was driven by a basic curiosity as to how hurricanes form from tropical waves. A practical outcome of PREDICT will be to provide forecasters with new quantitative metrics for evaluating the prospective development of easterly waves and other disturbances beyond 48 h.

SCIENTIFIC TOOLS USED DURING PREDICT. *Forecaster guidance.* The forecasting strategy for PREDICT consisted of three components. First, the observed state of the atmosphere was assessed from a "big picture" weather perspective using all available surface and upper air, satellite, and oceanic products, as well as all available numerical model guidance products. Candidate disturbances in the PREDICT domain (Fig. 1) were evaluated using these observational, satellite, and model products over the previous 48 h. Dropsonde observations obtained from the PREDICT GV research aircraft were used to help forecasters anticipate likely changes in convective organization of interest to PREDICT. During the time of peak activity in mid-September there were as many as five candidate disturbances simultaneously over the Atlantic Ocean and adjacent western seas.

After the big-picture weather perspective was completed and the information assimilated into the forecast process, PREDICT forecasters turned to the available numerical model guidance to evaluate the expected large-scale flow evolution and whether it would be favorable for the development or maintenance of tropical disturbances within the PREDICT domain over the next 120 h with emphasis on 0–72 h.

Sharpening the focus on candidate disturbances even further, the pouch products (see http://met.nps.edu/~mtmontgo/storms2010.html) were examined carefully for disturbances that exhibited recirculation in a comoving framework. Forecast model output was used to quantify the phase velocity of these disturbances in the lower troposphere over the 120-h forecast period. Typically, the procedure was to analyze the 700-hPa level. For cases with a pouch initially confined below 700 hPa, the 850- or 925-hPa levels were used.

Recirculation with a pouch is a necessary but not sufficient condition for development. Pouches with an initial value of the 700-hPa Okubo–Weiss (OW) parameter of at least $2 \times 10^{-9}\ s^{-2}$ that were forecast to grow and/or persist over the 120-h forecast period became potential targets for GV dropsonde missions to sample pregenesis and null disturbances. In simple terms, the OW parameter is a frame-independent measure of the tendency for a rotational flow to be shape preserving.[3] Mathematically, OW is defined here as $\mathrm{OW} = \zeta^2 - S_1^2 - S_2^2 = (V_x - U_y)^2 - (U_x - V_y)^2 - (V_x + U_y)^2$, where S_1 and S_2 denote strain deformation, ζ denotes vertical vorticity, (U, V) denote zonal and meridional velocity, respectively, and subscripts x and y denote partial differentiation in the zonal or meridional directions.

In formulating a strategy to determine which pouches should be sampled by aircraft, the science team needed to recognize that 1) westward-moving pouches had to reach at least 40 W before they would be in range of the GV, 2) disturbances within the PREDICT domain for multiple days would be of greatest interest, and 3) international air-traffic control constraints would limit flight operations in some regions bordering or extending into Haitian, Cuban, Venezuelan, or Colombian air space.

The forecast scenarios and strategies were discussed every day during the PREDICT forecast briefings held at 1400 UTC. The findings from this first briefing were shared with principal investigators (PIs) from the other agencies at 1500 UTC. This meeting of PIs provided a first opportunity to communicate each group's plan and explore possible avenues of collaboration. A tri-agency call at 1600 UTC, led on a revolving basis by forecasters from each group, provided a forum for all participants to view the day's forecast and flight plans. Similar meteorological information, including the pouch products, was used by all agencies (see companion paper by Evans et al. 2012 for further details).

Satellite products. From basic multispectral imagery, to specialized and experimental products, satellite data (both in digital and graphical form) played multiple important roles in PREDICT premission planning, forecasting, and real-time mission guidance. These data were also used extensively by the Genesis and Rapid Intensification Processes (GRIP) and Intensity Forecasting Experiment (IFEX) project teams and are a valuable asset to ongoing post–field phase analyses. Where available, the GV data will allow crucial in situ information to assess the accuracy and representativeness of these remotely-sensed products and derived fields.

The primary web portal for displaying satellite products and analyses for PREDICT was designed by the Cooperative Institute for Meteorological Satellite Studies (CIMSS) and the University of Wisconsin specifically to meet the needs of the field experiment similarly to what has been done for several projects in the past (Hawkins and Velden 2011). In addition to displays of basinwide imagery with large-scale product overlays, an interactive event-focused window allowed PREDICT analysts and forecasters to hone in on targets with greater detail. Selectable product overlays were available to interrogate the data and subtle mesoscale developments. The site can be found online at (http://cimss.ssec.wisc.edu/tropic2/predict). In particular, note the examples in the CIMSS Satellite Blog, put together by a CIMSS graduate student.

In addition to supporting the daily planning and forecasting, tailored satellite products were provided directly to the GV in real time during missions for in-flight analysis on the onboard display system. Hazard avoidance was a top priority of PREDICT flight managers, as the airplane was not designed to fly into highly turbulent regimes. Real-time displays of rapidly refreshed images of convection and overshooting tops (OTs) along with lightning overlays provided critical support in this regard [for an example of the CIMSS OT product display please see Fig. 2, and also the companion paper (Evans et al. 2012) for

[3] Assuming a scale separation between the slowly varying velocity field and the more rapidly varying field of squared vorticity (enstrophy), Weiss (1991) and McWilliams (1984) showed that positive values of OW indicate that the flow is vorticity dominant and shape preserving, whereas negative values of OW indicate a strain rate–dominated flow susceptible to rapid filamentation. A negative OW region is unfavorable for rotational organization of deep convection and aggregation of vortical remnants of prior convective activity.

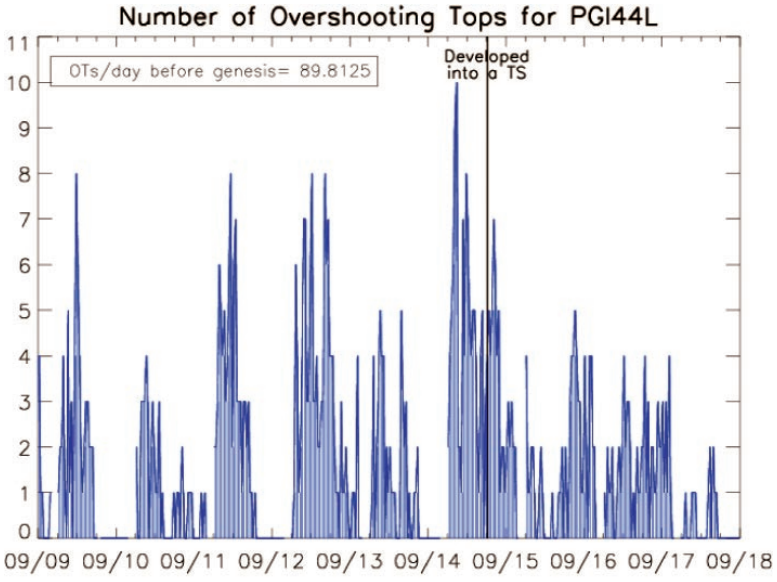

Fig. 2. Time series of overshooting tops derived from the CIMSS cloud-top product prior to and during the genesis of Karl (PGI44).

how the product can be useful to PREDICT scientific research]. The satellite data included key microwave images (Fig. 3) made available in near–real time by the Naval Research Laboratory group in Monterey via a specialized product collection and dissemination for PREDICT. The displays allowed onboard mission scientists to make crucial decisions on dropsonde locations, augmenting the analysis datasets to better meet the PREDICT science objectives.

To aid real-time guidance, the Geostationary Operational Environmental Satellite (GOES)-EAST satellite was put into rapid-scan operations (RSO) by NOAA/ National Environmental Satellite, Data, and Information Service (NESDIS) on several occasions at the request of PREDICT scientists. The more frequent image scans (every 7 min) provided for improved image interpretation of rapidly developing convection and circulations, and often allowed the pinpointing of smaller-scale circulation centers within the pouch. CIMSS used these images also to derive high-density and coherent atmospheric motion vectors (AMVs) to better define (quantitatively) the sub-synoptic and mesoscale flow features as the pouches evolved (see Fig. 4 for an example). From these winds, analyses of shear and other kinematic variables were derived for use both in real-time analysis and post-experiment case studies (daily examples can be found on the CIMSS PREDICT web page cited above).

As discussed in the foregoing section, the distribution of moisture is a key variable in the new model for genesis: both actively, as a necessary precursor

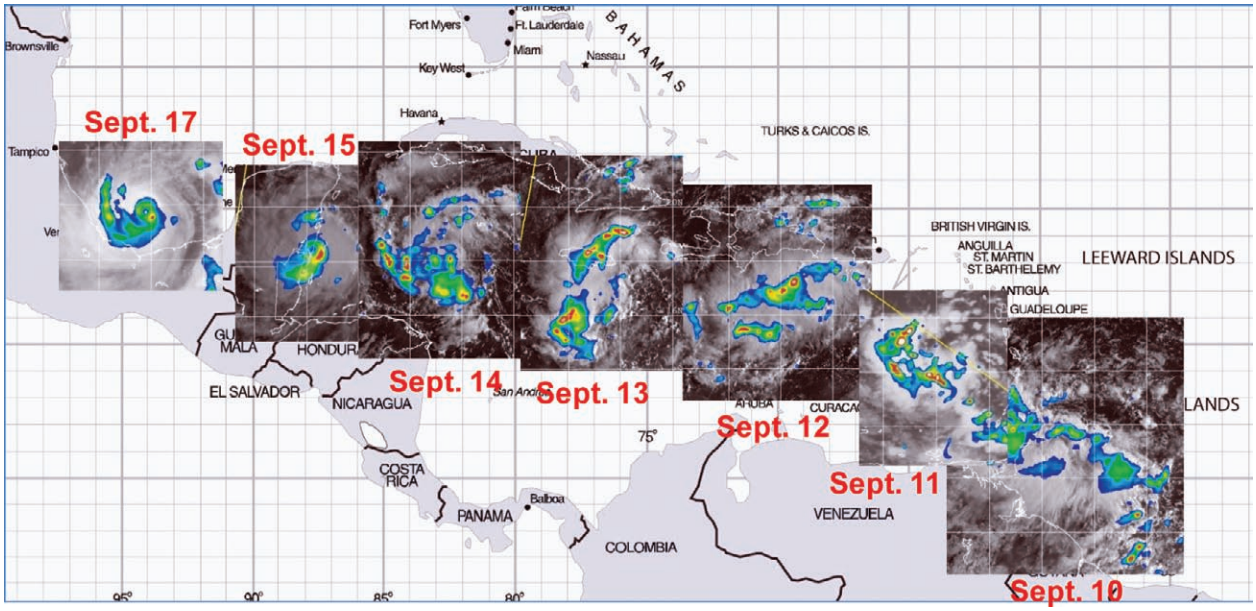

Fig. 3. 85-GHz montage (images courtesy of NRL-Monterey) for the active convection periods on each day from 10 to 17 Sep (excluding 16 Sep) during the genesis of Karl (PGI44). Note the small eye on the Yucatan coast on 15 Sep.

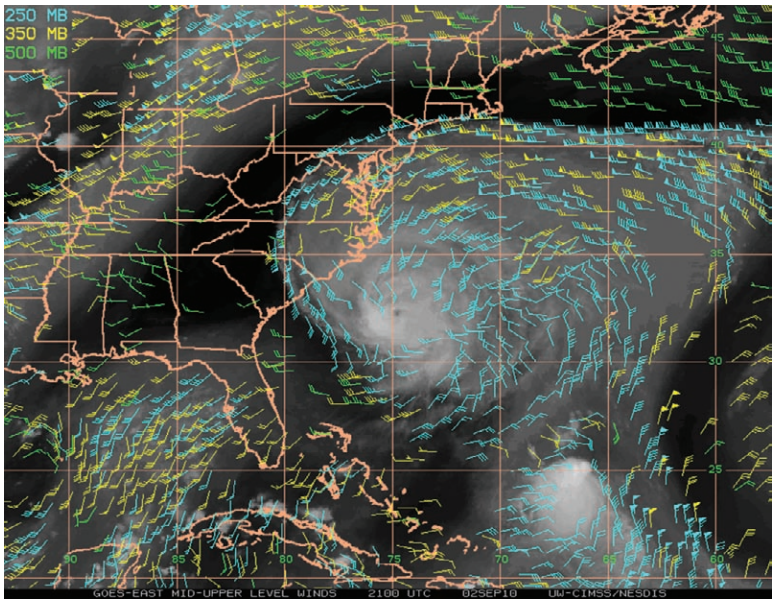

Fig. 4. Plot of upper-level satellite winds at 2100 UTC 2 Sep 2010. The image is centered on Hurricane Earl, with its upper-level outflow producing an impinging vertical shear on Tropical Storm Fiona (formerly PGI36), located east of the Bahamas.

to saturate the column near the pouch center via aggregate convection, and passively, as a tracer to spot entrainment, if any, of dry air into or over the core that can disrupt the genesis process. CIMSS developed a total precipitable water (TPW) product based on morphing microwave sensor data from multiple polar-orbiting platforms (Wimmers and Velden 2007, 2011). An animated, basin-scale product ran continuously during PREDICT and was used every day to assess the large-scale moisture conditions and trends. In addition, an experimental product was developed to show the TPW in a comoving frame. An example is shown in Fig. 5, just a few hours after a GV mission into ex-Gaston (http://cimss.ssec.wisc.edu/tropic/realtime/tpwROI/ROIs/PGI38L/web/display04W.html) and suggests plausibly how the pouch resists the environmental dry air to the west and sustains a moist core, at least for 2–3 days in this case. The overlain vectors show the system-relative flow (with the parent wave's phase speed subtracted) of the lower-tropospheric mean wind as deduced from Global Forecast System (GFS) wind analyses. This product illustrates the recirculating flow and trapped moisture in the pouch in the comoving framework and will serve as an analysis tool to further assess the new cyclogenesis model.

Another valuable source of moisture analysis is the suite of satellite-derived products to detect the Saharan air layer (SAL). This air mass is considered hostile to Atlantic tropical cyclones (Dunion and Velden 2004; Evan et al. 2006; Jones et al. 2007; Wu 2007; Dunion and Marron 2008; Sun et al. 2009; Reale et al. 2009; Shu and Wu 2009), primarily due to the characteristically very dry and dusty midlevel air. Satellite-derived products designed to depict the SAL based on multispectral approaches to isolate the dust and dry air effects on radiances are available during the PREDICT period (i.e. the CIMSS main tropical cyclones website archive). A contentious issue regarding the influence of the SAL on Atlantic TC development is whether the dry air actually gets into the core to disrupt the convection structure. The NOAA/Hurricane Research Division (HRD) SAL Experiment (SALEX) missions flown over the past few years are attempting to document this. Certainly, the PREDICT flights will augment this database to provide further information on the SAL–TC interaction.

All of the satellite data and products collected during PREDICT were disseminated to the NCAR Earth Observing Laboratory (EOL) field program support facility in Boulder, Colorado, for permanent and free-access archiving.

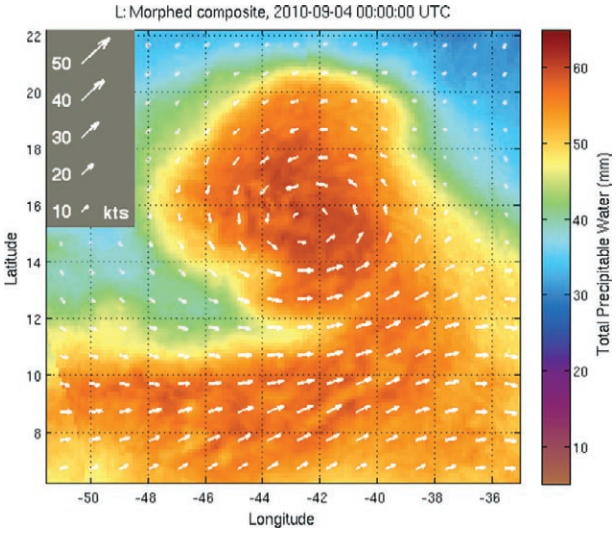

Fig. 5. Mosaic of total precipitable water (TPW, in mm) and system-relative winds at 850 hPa (vector scale, top left, in kt) valid 0000 UTC 4 Sep, approximately 4 h after the GV concluded its second mission into PGI38 (ex-Gaston).

"Pouch products" for GV flight planning (days −1 to −3). During the field experiment, the sweet spot for TC formation (defined as the intersection of trough axis and critical latitude) derived from global model forecasts was considered as the potential target of research flights. Each day, for each pouch observed at the forecast initial time, a pouch's "vital signs" (see the Internet link for pouch products in the previous "forecaster guidance" section) and center track were calculated and examined based on the 5-day forecasts from the European Centre for Medium-Range Weather Forecasts (ECMWF), GFS, the Met Office (UKMET), and the Navy Operational Global Atmospheric Prediction System (NOGAPS). A consensus pouch track was formulated also. Operational constraints for most of PREDICT required the depiction of a pouch in the comoving fields (consistent with the new model) of at least one of the global models at analysis time in order to begin tracking a new system (DMW09). By the end of the experiment, however, we were occasionally initiating tracks of vorticity or OW maxima that did not initially exhibit a clear recirculation region in the analysis, but were forecast to do so within a day or so. Each tracked system was assigned a number (beginning at the start of June prior to PREDICT) preceded by the letters PGI, which stand for the three projects ongoing during the 2010 Atlantic hurricane season: PREDICT, GRIP, and IFEX.

The "pouch tracks" were all plotted atop GOES TPW and other diagnostic variables (i.e., 850-hPa relative vorticity, upper-level divergence, etc.) by the CIMSS/University of Wisconsin team. Then a flight pattern was designed based on the pouch track to sample the disturbance over a spatial range of approximately 500 km × 500 km centered on the pouch position and over a time period of 4–6 h.

Karl, a well-surveyed case during PREDICT, serves as an illustrative example. The GV sampled pre-Karl (PGI44) for five consecutive days from 10 to 14 September. During the PREDICT midday coordination sessions on 13 September, the pouch products based on ECMWF forecasts from 0000 UTC 13 September were available for planning the following day's flight. ECMWF 36-h forecasts depicted a trough located along 82°W at the flight time of 1200 UTC 14 September. In an Earth-relative frame, the circulation center as depicted by 700-hPa streamlines was at about 17.3°N and situated on the southern edge of a large region of positive values of the OW parameter (Fig. 6, left). The circulation in the comoving frame (Fig. 6, right) is better defined than in the Earth-relative frame. The 700-hPa Earth-relative flow

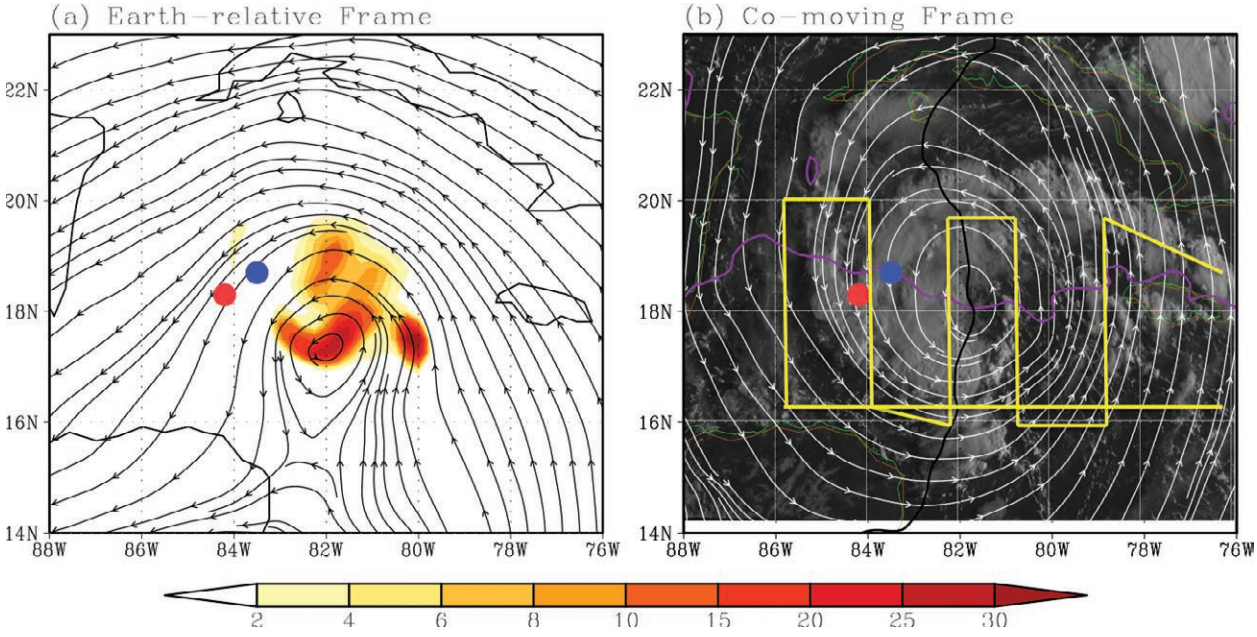

Fig. 6. (left) ECMWF 36-h forecast of 700-hPa Earth-relative streamlines and OW (shading; units: 10^{-9} s^{-2}) centered on wave pouch PGI44/AL92 (pre-Karl) valid at 1200 UTC 14 Sep 2010. (right) Streamlines in the co-moving frame of reference (phase speed of 6.2 m s^{-1} westward), GOES visible imagery at 1225 UTC, and flight pattern of GV aircraft (yellow track). In the right figure, the black curve represents the trough axis and the purple curve the local critical latitude defined by $U = c\_x$, where c_x denotes the wave's zonal phase speed. The red dot represents the actual genesis location, and the blue dot is the ECMWF 700-hPa predicted sweet spot, defined by the intersection of the trough axis (black curve) and critical latitude (purple curve), at 2100 UTC 14 Sep 2010.

depicts a tropical wave with an inverted-V pattern and only weak westerly flow south of the vortex. The circulation center in the comoving frame of reference is located between two areas of high OW (Fig. 6, left) that appear to be wrapping around the pouch center. A large lawnmower pattern was constructed that sampled both Earth-relative and comoving circulations and a region beyond the central convection.

As described during the PREDICT weather briefing at 1400 UTC 13 September, the CIMSS-PREDICT "invest" page showed that the disturbance was associated with weak deep-layer shear (5–10 kt), a strong lower-tropospheric vorticity maximum embedded in high TPW values, a corridor of high SSTs (29°–30°C) along the track of the ECMWF forecast pouch, and convective banding in the visible/infrared (VIS/IR) satellite imagery. At 2100 UTC 14 September, the National Hurricane Center (NHC) declared the disturbance Tropical Storm Karl at 18.3°N, 84.2°W (the red dot in Fig. 6). This position is quite close to the forecast sweet spot (18.7°N, 83.5°W) at the same time (the blue dot in Fig. 6).

Ensemble weather forecast products. During the field phase, daily forecast products derived from operational global Ensemble Prediction Systems, experimental regional-scale ensemble analyses, and related forecasts augmented short- and long-range planning activities. In future research, these ensemble systems will address hypotheses related to the predictability of genesis, the sensitivity of predictions to enhanced observations, and physical insight into the genesis process. For example, the potential development of pre-Karl (PGI44) was identified in the global and mesoscale model ensembles between 5 and 10 days before its officially declared genesis late on 14 September. In the 9-day ECMWF ensemble forecast, the probability of the lower-tropospheric relative vorticity (averaged within a disk of radius 300 km) attaining its verified value at the onset of genesis (5.65×10^{-5} s^{-1}) was still low in the broad region in which Karl was to develop (Fig. 7). In contrast, for the corresponding 7-day forecast initialized two days later, a cluster of solutions of varying strengths, including some consistent with a tropical storm, was evident in the Caribbean (Fig. 7a) with a very different probability distribution (Figs. 7b,c).

For short-range (24–72 h) guidance, two experimental mesoscale ensemble forecast systems were run also during the field phase. The first system was a cycling, mesoscale-ensemble Kalman filter, similar to what is described in Torn (2010) using the Advanced Research Weather Research and Forecasting (WRF) model (Skamarock et al. 2005). This system assimilated conventional in situ data, tropical cyclone (TC) position and minimum sea-level pressure (SLP), Global Positioning System (GPS) radio-occultation estimates from the Constellation Observing System for

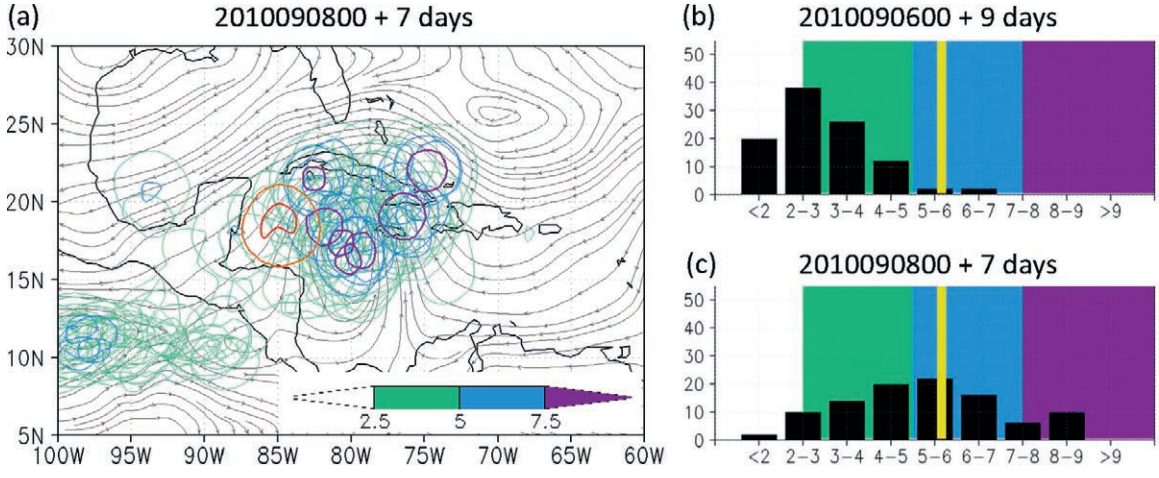

Fig. 7. (a) 7-day, 50-member ECMWF ensemble predictions for PGI44 (pre-Karl), initialized at 0000 UTC 8 Sep 2010, of relative vorticity averaged over the 700–850-hPa layer and an area of radius 300 km. Contours of 2.5, 5, and 7.5 × 10^{-5} s^{-1} are illustrated. The corresponding ECMWF analysis at 0000 UTC 15 Sep 2010 is given by the orange (2.5 × 10^{-5} s^{-1}) and red (5 × 10^{-5} s^{-1}) contours. (b),(c) Probability distribution function (PDF) of maximum averaged relative vorticity within a box of 12°–24°N, 90°–70°W for (b) 9-day ECMWF ensemble forecast initialized at 0000 UTC 6 Sep 2010 and (c) 7-day ECMWF ensemble forecast initialized at 0000 UTC 8 Sep 2010. The shaded colors correspond to the contour values in (a), and the verifying value of 5.65 × 10^{-5} s^{-1} in the ECMWF analysis at 0000 UTC 15 Sep 2010 is given by the vertical yellow line.

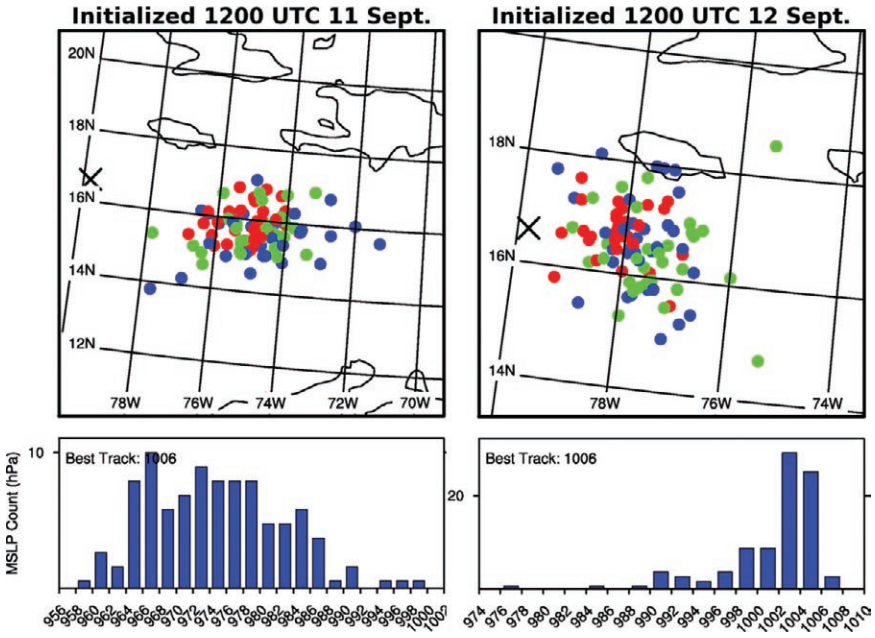

Fig. 8. Ensemble forecasts of (top) PGI44's position and (bottom) minimum sea level pressure initialized (left) 1200 UTC 11 Sep and (right) 1200 UTC 12 Sep 2010 valid 0000 UTC 14 Sep. The red (blue) dots denote the 1/3 of members with the lowest (highest) minimum SLP, while the green dots denote the middle 1/3 of members. The X denotes the verification position.

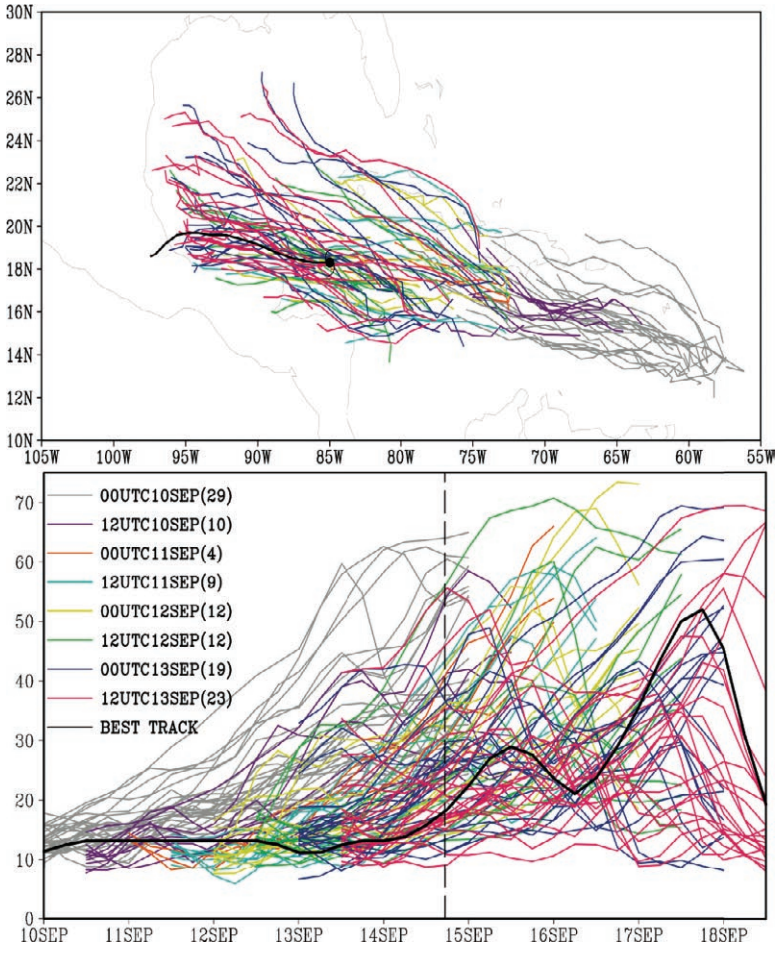

Meteorology, Ionosphere, and Climate (COSMIC) array of satellites (e.g., Anthes et al. 2008), and dropsonde data. A 12-km mesh following any disturbance designated by NHC as an INVEST[4] (or stronger) was nested in a basin-covering 36-km domain. At 0000 and 1200 UTC each day, all 96 ensemble analyses from this system were integrated out 72 h in order to permit the evaluation of mesoscale probabilistic products and initial condition sensitivity calculations (e.g., Torn and Hakim 2008).

Figure 8 shows the forecast of PGI44 (pre-Karl) at 0000 UTC 14 September initialized at two different times. Whereas the earlier forecast is characterized by larger variance in both the position and minimum SLP, the latter forecast has a tighter probability distribution and is closer to the verification values. The differences in these forecasts likely results from the assimilation of dropsondes from the GV, although further numerical experiments are needed to confirm

[4] The term INVEST is used by operational tropical cyclone forecast centers to identify an area of interest for collection of specialized observations or running model guidance. The designation of a system as an INVEST does not correspond to a likelihood of development (NHC 2010).

Fig. 9. Track and intensity forecasts of PGI44 (pre-Karl) by eight consecutive sets of 30-member 4.5-km 120-h WRF ensemble forecasts initialized from the PSU real-time hybrid EnKF analysis. Only ensemble members that reach the intensity of TC genesis are plotted with the number of members at different times shown in the bracket.

this. At both initialization times, there is a slight tendency toward the more intense cyclones being farther west.

The other limited-area ensemble prediction system run at The Pennsylvania State University (PSU) was based on a different cycling mesoscale-ensemble Kalman filter (EnKF) (Meng and Zhang 2008a,b; Zhang et al. 2009). The 60-member ensemble system assimilated all nonradiance data used in the National Centers for Environmental Prediction (NCEP) global model on two fixed outer domains centered on St. Croix (with grid spacings of 40.5 and 13.5 km). A vortex-following nest of 4.5-km grid spacing was added for forecasts that were integrated out to 120 h.

Figure 9 shows the track and intensity forecasts of pre-Karl by eight consecutive sets of forecasts initialized every 12 h from 0000 UTC 10 September to 1200 UTC 13 September. Of the 30 members in each ensemble forecast, the number of members that reached tropical storm strength was 29, 10, 4, 9, 12, 12, 19, and 23 in successive forecasts. Earlier forecasts developed Karl too soon, but this error was reduced in subsequent cycles. Thus, the intensity forecasts in both regional ensemble systems were similar in the case of Karl. The ensemble of tracks maintained a similar spread through time and were approximately evenly distributed around the observed track of Karl.

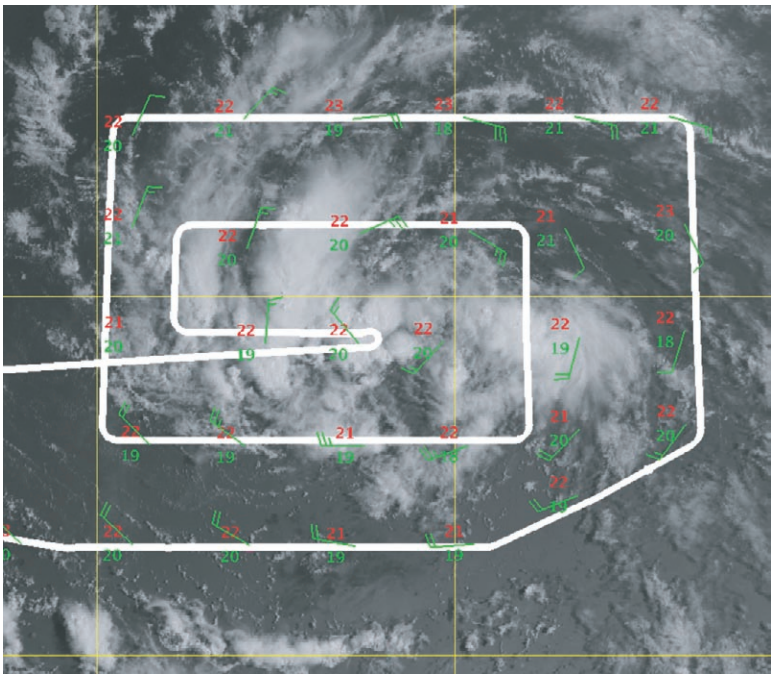

Fig. 10. Dropsondes and flight track from the first GV flight into PGI36 (soon after designated Tropical Storm Fiona by NHC) on 30 Aug. Shown are wind, temperature (red), and dewpoint (green) at 900 hPa centered roughly on 1300 UTC. The flight track is indicated by the thick white line segments. GOES visible satellite image is from 1315 UTC.

TROPICAL DISTURBANCES OBSERVED DURING PREDICT. The tropical predepression environment presented many challenges for research flight operations during PREDICT. The GV is a high-performance aircraft that was not designed to penetrate deep convection, but observations were desired in and around the convection within and on the periphery of the pouch. The "square-spiral" flight plan (see Fig. 10) proved to be one of the most successful patterns during the experiment, enabling careful monitoring of developing deep convection as the aircraft spiraled in to the center of the pouch while steadily gaining altitude. Visual, radar, and satellite estimates of convective activity were generally in good agreement, providing confidence that the GV's altitude was high enough to fly above most cloud tops and obtain comprehensive spatial coverage throughout a predepression target.

The scientific tools summarized in section 3 helped the scientists in the operations center devise accurate flight plans and guide the GV safely through a dynamic environment. Updated information about the evolving meteorological situation was available through a satellite data link, assisting the pilots and mission scientists with in-flight decision-making to improve the quality of the research data collection. All scientists on board were able to customize their own data displays to focus on the measurements of interest being collected in real time. Scientists in the operations center were able also to see much of this information and could collaboratively adjust the flight patterns with the flight crew in real time when necessary.

Apart from the first flight, a test mission on 15 August, the remaining 25 PREDICT missions examined a variety of disturbances. Figure 11 and Table 2 summarize the systems that were investigated. The nomenclature used to identify disturbances during PREDICT was PGIXX, where XX is the number assigned to a system, retained during its identifiable lifecycle, and PGI is an abbreviation for PREDICT–GRIP–IFEX. This number differs from

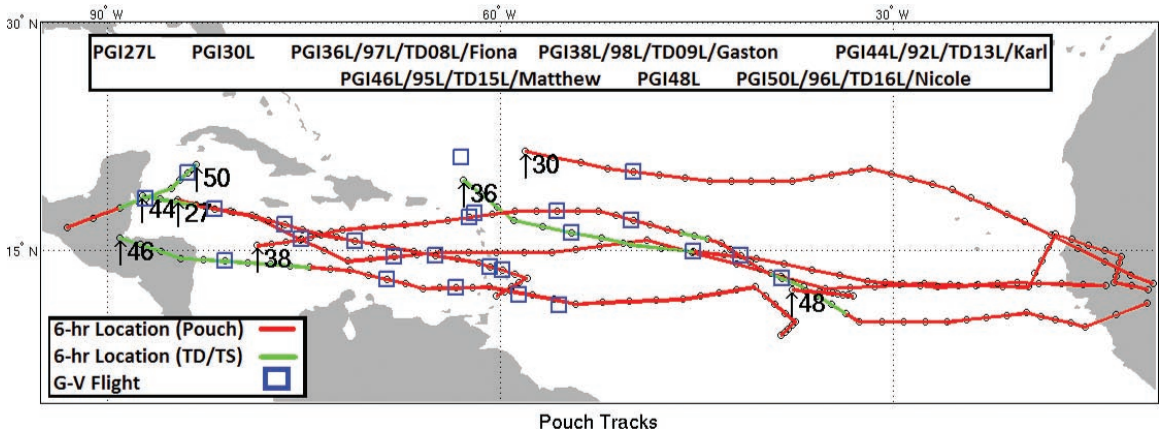

Fig. 11. Pouch tracks for systems that were flown by the GV during PREDICT. The values at the track endpoints indicate the PGI number designations.

Table 2. Disturbances investigated with the GV, along with origin of predepression disturbance, date "pouch tracking" began, date of first mission, date and time of genesis as declared by NHC (if it occurred), number of GV missions and days flown, and number of successful dropsondes.

SYSTEM	Description	First identification	First mission	First NHC advisory	Flights (days)	Drops
PGI27	Nondeveloping African wave	8 Aug	17 Aug	None	2 (2)	48
PGI30	Nondeveloping African wave	14 Aug	21 Aug	None	2 (2)	38
PGI36 (Fiona)	Developed African wave	25 Aug	30 Aug	2100 UTC 30 Aug	3 (3)	83
PGI38 (ex-Gaston)	Failed redevelopment of African wave	28 Aug	2 Sep	1500 UTC 1 Sep	5 (5)	109
PGI44 (Karl)	Developing non-African wave	9 Sep	10 Sep	2100 UTC 14 Sep	6 (5)	127
PGI46 (Matthew)	Developing wave of uncertain origin	16 Sep	20 Sep	1800 UTC 23 Sep	4 (4)	83
PGI50 (Nicole)	Developing Caribbean gyre	26 Sep	28 Sep	1500 UTC 28 Sep	2 (2)	47
PGI48	May have become Otto	26 Sep	30 Sep		1 (1)	26

and generally preceded the operational designation by the NHC, whether an INVEST (e.g., 9xL) or tropical depression (e.g., TD1, TD2, etc.). In the case where a storm became a tropical depression or stronger as designated by NHC, it was known by both its PGI number and the official tropical depression number (or storm name).

The storms sampled by PREDICT aircraft missions were fairly evenly split between developing and nondeveloping systems (see Table 2 for details). While some cases had a high potential for genesis from the time of the first GV flight into them and subsequently developed, one system departed from this pattern. Gaston was a surprising instance where development occurred initially, but following a period of decline (sampled by the GV) redevelopment did not occur. PGIs 27 and 30 were null cases as anticipated from the time of the first GV mission, but Matthew (PGI46) surprisingly formed in only three days from a weak disturbance in the mid-Atlantic ITCZ. In the remainder of this section, each of the eight observed disturbances will be summarized along with a few preliminary analyses to assess the nondevelopment of Gaston in comparison with the developing case of Karl.

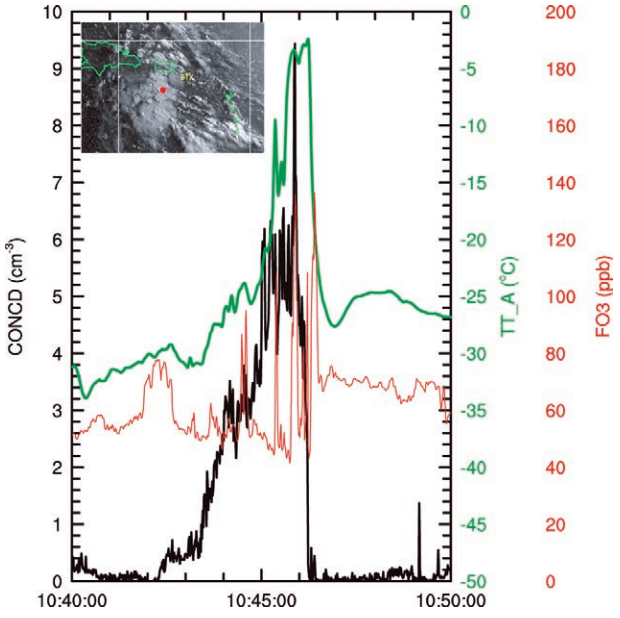

Fig. 12. Time series of small ice particle concentration (CONCD, black curve), total air temperature (TT_A, green curve), and ozone mixing ratio (FO3, red curve) during the encounter with a high-IWC region penetrated during RF02. The satellite image, valid at 1045 UTC, is shown at upper left with the location of the GV indicated by the red dot at this time.

1) *PGI27.* PGI27 was first detected near the west coast of Africa on 8 August as a low-amplitude easterly wave. It traversed the tropical Atlantic with a ground-relative speed of 8–9 m s^{-1} westward. Organized deep, moist convection was evident on 16 August and the first flight of the GV was on 17 August. On this flight (RF02) the GV encountered several regions of high ice water content (IWC). These are of intrinsic scientific interest (e.g., Herman and Heymsfield 2003), and they are also regions of concern for aviation safety. The duration of the most substantial high-IWC penetration was 172 s corresponding to a horizontal path of 40 km, at an altitude of 13 km (Fig. 12). The high-IWC region was penetrated about 2 km below the tropopause at a temperature of about −58°C. At the time of the aircraft penetration, GOES IR imagery showed that this was a region of developing convection with an anvil of about 100 km across (Fig. 12). Ice particle concentration peaked at nearly 10 cm^{-3} [CONCD; 2–50 micron, from a Cloud Droplet Probe (CDP) manufactured by Droplet Measurement Technologies, Boulder, Colorado]. As a consequence of the ingestion of high IWC, the temperature sensors filled with ice. The built-in heaters melted part of the ice, and meltwater ran onto the temperature sensor elements, bringing the recorded (total) air temperature to near 0°C (TT_A, from the avionics system). Measurements of ozone concentration show the high IWC region as characterized by values around 40–50 ppbv, but with peaks of >80 ppbv. These peaks indicate mixing with upper tropospheric and/or stratospheric air. On the following days, PGI27 did not develop; the reasons are not yet clear but may include lack of a well-defined recirculating flow and dry air intrusion.

2) *PGI30.* PGI30 was a very weak tropical wave featuring only a tiny area of deep convection (cloud-top temperature of −60°C occupying an area less than 2,500 km^2) near the center of a pouch with minimal circulation strength. Convection did persist, episodically, in this region following the wave. Two missions were flown into PGI30, on 21 and 23 August, partly to investigate a case that was clearly a nondeveloper and partly to test the GV dropsonde system, which was experiencing some problems at the time.

3) *Fiona.* In contrast to PGI30, pre-Fiona was a strong wave as it moved off the African coast on 27 August at roughly 9 m s^{-1} westward. At the time of the first GV mission on 30 August (centered on about 1300 UTC), Fiona was officially still an INVEST (97L) but was upgraded to a tropical storm based on the GV dropsondes (Fig. 10), which indicated a well-organized cyclonic circulation, as well as on satellite images showing banded precipitation features (see NHC storm report by Robbie Berg at www.nhc.noaa.gov).

Subsequent flights into Fiona occurred on 31 August and 1 September as the storm strengthened slowly but did not reach hurricane intensity. It is hypothesized that some inhibition of development may have resulted from the vertical shear created by the anticyclonic outflow of Hurricane Earl to the northwest of Fiona (Fig. 4). Convection became highly asymmetric, focused on the south (downshear) side of the vortex during this period. Fiona's pouch was subject to Earl's strain deformation as well.

4) *Gaston.* Our attention then turned to Gaston, which developed from the African wave following the wave that became Fiona. This system was declared a tropical storm by NHC at 1500 UTC 1 September. However, dropsondes from the GV deployed during its first mission into Gaston indicated that the storm had weakened to a tropical depression and Gaston was officially downgraded to an INVEST.

The distribution of moisture was a critical aspect in the evolution of ex-Gaston. Two sources of in situ water vapor profiles were obtained from the GV. The Global Navigation Satellite System Instrument System for Multistatic and Occultation Sensing (GISMOS)

was developed for the GV to perform airborne GPS radio occultation (GPS RO) measurements (Garrison et al. 2007; Xie et al. 2008). This measurement technique is based on the same principle as the COSMIC radio occultation profiles used in the WRF ensemble Kalman filter model mentioned above. GPS RO is a limb-sounding technique that senses the atmosphere using radio signals that traverse the atmosphere as a transmitting GPS satellite sets behind the horizon relative to a moving receiver. The radio wave undergoes refractive bending and a Doppler shift due to variations of refractive index. Retrieval techniques that assume spherical symmetry of the atmosphere map the refractivity variation to the height at the point of closest approach to Earth, referred to as the tangent point. This horizontal position of the tangent point varies with altitude; hence, the vertical refractivity profile is slanted along a horizontal distance of approximately 100–300 km (Fig. 13). Retrievals of water vapor from the observed refractivity are being developed. Future work plans to test the usefulness of these observations in simulating the failure of ex-Gaston to redevelop.

Another perspective on the role of moisture within the pouch of ex-Gaston can be obtained by comparing the thermodynamic structure of ex-Gaston with that of a developing disturbance (pre-Karl to be discussed in more detail below). The day-to-day evolution of the "pouch-mean soundings"[5]obtained from the GV dropsondes during missions into ex-Gaston and the system that finally became Karl are shown in Figs. 14a and Fig. 14b, respectively. These mean pouch soundings are characterized by the virtual potential temperature (θ_v) and pseudo-equivalent potential temperature (θ_e) as a function of height. Features that stand out include the following:

- There is little difference in the day-to-day variation in θ_v, either in the developing or the nondeveloping system.
- There is a general increase in the lower tropospheric θ_e in both systems, but the increase is not monotonic for Karl.
- In the nondeveloping system there is a decrease in the midtropospheric θ_e, whereas this quantity increases a little in the developing system.
- At the end of the observation period for each disturbance, there is a much larger difference between the near-surface θ_e and the midtropospheric θ_e minimum in the nondeveloping system (~25 K) compared with the difference in the developing system (~17 K).

According to traditional reasoning, the last feature would have implications for the strength of convective downdrafts, which on the basis of these soundings would be expected to have been larger in the nondeveloping system (e.g., Emanuel 1994). The argument is that stronger downdrafts (normally attributed to the lower midtropospheric relative humidity) would tend to import low θ_e into the boundary layer, offsetting the enhancement of boundary layer θ_e by sea-to-air moisture fluxes. This enhancement is necessary to fuel subsequent deep convective activity. Persistent deep convection is a prerequisite for genesis through its role in vortex tube stretching and thereby local vorticity generation in the lower

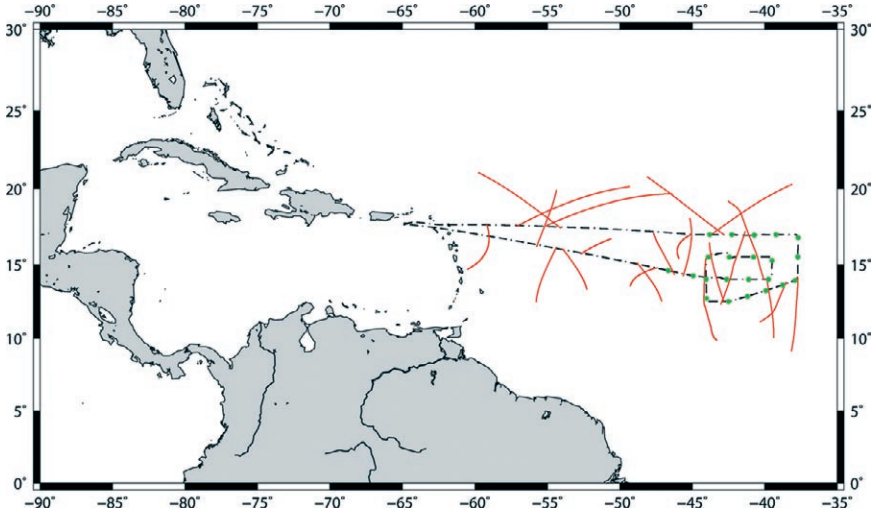

Fig. 13. GV flight track (dot–dashed line), dropsonde locations (green), and horizontal locations sampled by the slanted occultation profiles recorded on 3 Sep during the second mission into PGI38 (ex-Gaston). Recordings are made continuously during ferry flights as well, in this case sampling the upstream environment of PGI38.

[5] The pouch-mean sounding was derived here provisionally by averaging all soundings of a day's mission with a total precipitable water content larger than 50 kg m^{-2}. This criterion was found to correspond roughly with the region of closed streamline contours at 700 mb in the ECMWF analysis near the time of the mission and eliminated only a small fraction of soundings on the periphery of the system.

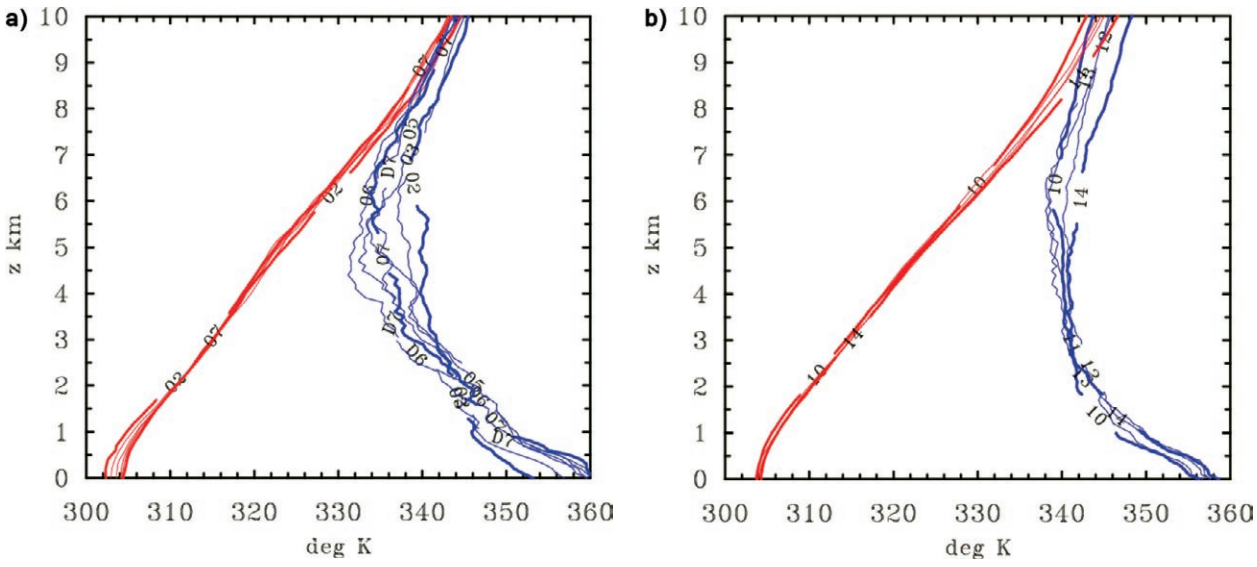

Fig. 14. Comparison of pouch-mean soundings of virtual potential temperature (θ_v) (red) and pseudo-equivalent potential temperature (θ_e) (blue) as a function of height derived from the NSF GV and NASA DC8 dropsondes in (a) the pouch of PGI38 (ex-Gaston) that failed to redevelop and (b) the pouch of PGI44 (pre-Karl) that did develop. Numbers on curves refer to the day of the flight mission in Sep 2010. The thick curves mark the first and last days of the GV flights. Curves for the NASA DC8 flights are denoted with the prefix D.

troposphere (Montgomery et al. 2006; Montgomery and Smith 2010).

A more recent view on the role of midlevel dry air has emerged from numerical simulations using cloud models (James and Markowski 2010; G. Kilroy 2011, personal communication). These studies suggest that the principal effects of the dry air are to reduce the updraft strength and water loading, while the downdraft strength is not changed appreciably. The reduction of latent heat release leads to a reduction in cloud buoyancy, thereby rendering the clouds less effective in amplifying vertical vorticity. More extensive comparisons of the thermodynamic aspects of developing and nondeveloping disturbances in the PREDICT experiment are presented in Smith and Montgomery (2011).

As to the source of this drier air in Gaston, there is evidence of a strong, dry Saharan air mass surrounding the northern hemisphere of Gaston in multiple satellite-derived products (discussed in the section "Satellite products" on p. 173 of this issue). In addition, dropsonde thermal and moisture profiles do resemble the SAL-type soundings identified in Dunion (2011). However, further analysis is required to determine the contribution of this air mass to the dry air seen in the dropsonde observations.

Dry air continued to plague ex-Gaston during the subsequent days. The cyclonic circulation became shallower over time also. By 5 September, the circulation was not evident at 500 hPa and by 7 September it was barely evident at 700 hPa. The storm continued to produce intense convection intermittently throughout the period, but the vortex systematically weakened.

5) *Karl.* The pre-Karl disturbance, PGI44 (defined above), originated within the ITCZ region near the northern coast of South America. A surge of southwesterlies over northern South America around 8 September locally strengthened the ITCZ between 50° and 60°W and resulted in the formation of a quasi-persistent area of convection along the ITCZ near the northern coast of South America. An easterly wave formed subsequently near this locale and propagated westward towards the eastern Caribbean.[6] Convection within the early pre-Karl disturbance was elongated east–west on 10 September (Fig. 3). On this day, PREDICT utilized two crews to conduct two missions, one centered on roughly 1300 UTC and the other about 6 h later. Both flights revealed a broad gyre of diameter roughly 400 km that featured similar tangential winds between 900 and 500 hPa.

[6] The marsupial framework includes in situ wave formation via hydrodynamic instability of the ITCZ, in addition to neutral wave propagation across the basin (DMW09).

Pre-Karl was rather slow to develop over the next several days. Although not as pronounced as observed in the pouch of Gaston, the minimum θ_e observed in the composite soundings shown in Fig. 14b are believed sufficient to support a pronounced diurnal cycle and boundary layer recovery from 9 to 13 September, with the maximum intensity of convective updrafts (as judged by the CIMSS overshooting top product in Fig. 2) occurring around 1200–1500 UTC (late morning local time). Over the course of 11–14 September, convective activity consolidated from an initial southwest–northeast elongation to a more compact pattern encircling the sweet spot within the pouch (Fig. 6), the latter being close to the location where Karl formed later on 14 September. An interesting aspect of Karl is that, despite the large-scale initial circulation, the storm that actually formed was small (Fig. 3).

6) *Matthew.* In contrast with Karl, Matthew was generally unforeseen as few as 5 days prior to its formation. While the PREDICT team was tracking weak vorticity features connected with the ITCZ on 17 and 18 September, it was not until deep convection erupted near the analyzed sweet spot on 19 September that there was a feature sufficiently defined in the atmosphere and in global models to plan a mission. The first GV mission was time-centered roughly on 1600 UTC 20 September. At this time, the pre-Matthew disturbance was as weak as PGI27 in terms of the average tangential wind within 300 km of the lower tropospheric circulation center and appeared less organized than Karl at the time of the first mission. However, Matthew quickly organized on 21 and 22 September.

Figure 15 indicates that the pouch was well defined on the 22nd with strong convection occurring close to the predicted maximum in OW and sweet spot in the analysis from the ECMWF model. Matthew went on to develop into a strong tropical storm on 23 September, but despite forecasts of potential rapid intensification it did not intensify further and made landfall in Belize as a moderate tropical storm late on 24 September. Despite many similarities to Karl in its midocean origin and track through the Caribbean, Matthew developed rapidly, but it failed to become a hurricane whereas Karl developed slowly and eventually formed into a major hurricane.

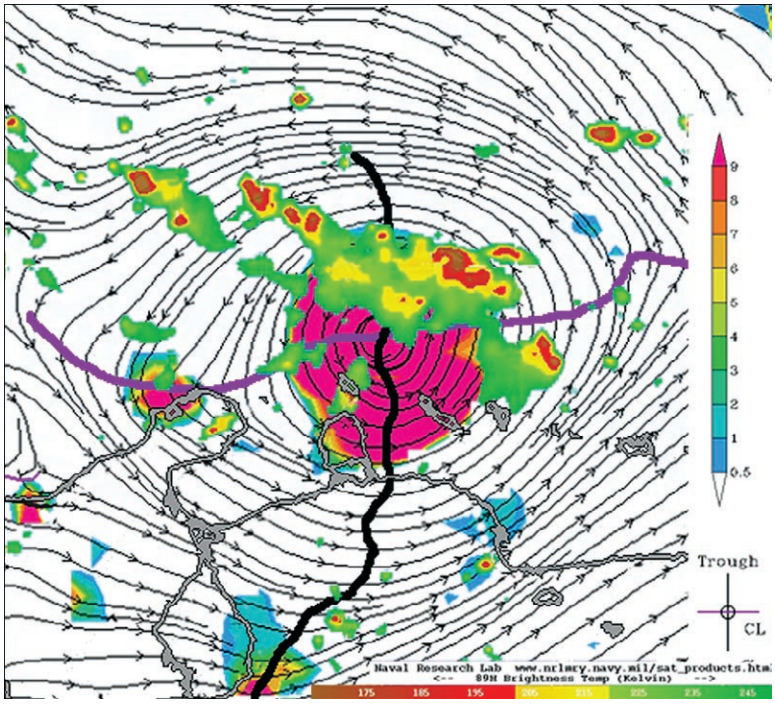

Fig. 15. Comoving streamlines (light grey) and regions of positive OW with cyclonic vorticity (light blue and purple; color bar units of 10^{-9} s^{-2}) at 700 hPa at 1200 UTC 22 Sep derived from the ECMWF analysis. Superposed on these fields are Advanced Microwave Scanning Radiometer for Earth Observing System (AMSR-E) 89-GHz brightness temperatures (units of K; green, yellow, and red) from the 1818 UTC overpass. The pouch sweet spot, defined by the intersection of the trough axis (thick black curve) and critical latitude (CL; thick purple curve), is highlighted by the light black circle. AMSR-E brightness temperature is courtesy of NRL-Monterey. South American landmass and adjacent islands are outlined by the thick grey curves.

7) Nicole. In the wake of Matthew a large gyre formed over Central America in which strong flow from the eastern Pacific extended across Panama and Costa Rica into the Caribbean. The NHC initiated a tropical depression advisory to the east of Belize on the eastern side of this gyre at 1500 UTC 28 September. The tropical depression tracked northeastward and became a weak tropical storm (Nicole) at 1500 UTC 29 September over central Cuba. Tropical storm Nicole tracked north-northeastward and dissipated subsequent to 2100 UTC 29 September in the Florida Strait.

The pregenesis environment of Nicole was interesting because the storm appeared to originate out of a broad area of multiple low-level vorticity maxima that stretched from

the Gulf of Tehuantepec to the Bay of Campeche and then eastward across northern Guatemala and Belize to the southwestern Caribbean Sea. The presence of multiple low-level vorticity maxima on the east side of the larger gyre created great uncertainty in properly locating pouch PGI50. Model (GFS, ECMWF, UKMET, NOGAPS) uncertainty on the forecast track, duration, and intensity of Nicole was perhaps the largest of any TC during PREDICT. The Nicole case is of scientific interest for several reasons. First, what role did Matthew's pouch play in establishing this gyre complex? Second, did other disturbances from the east enter this region and influence the development of Nicole? Third, how does a developing system emerge from within a larger gyre complex possessing multiple low-level vorticity centers, with or without the support of a parent wave in the lower troposphere above the boundary layer? Fourth, this case provides an excellent test bed for TC genesis predictability experiments. Noteworthy is that the ECMWF ensemble anticipated the development of a major circulation center in this region 10 days in advance.

8) PGI48 (pre-Otto?). The final mission of PREDICT was flown on 30 September the final day of the project. The target was a weak circulation centered near 13°N, 57°W associated with relatively disorganized convection across an area of nearly 1,000 km. The circulation drifted northwestward over the following several days and may have become entwined in the development of Hurricane Otto, a tropical transition event (Davis and Bosart 2004), on 5 October.

LESSONS LEARNED AND THE ROAD AHEAD. While we anticipate that many research findings will arise from the careful analysis of PREDICT observations (in conjunction with observations taken during GRIP and IFEX), there were some clear lessons learned that are summarized here. First, the GV's ability to fly quickly to the target region at high altitude and safely navigate over or around deep convection proved that this sampling method, incorporated in the PREDICT proposal strategy, is highly effective for investigating tropical cyclogenesis in remote oceanic areas.

Another lesson learned is that tropical cyclogenesis may be more predictable than previously thought. PREDICT demonstrated that genesis regions could be targeted more than 2 days in advance, and in some cases 4-day projections were useful. This is not to say that genesis itself was predictable on longer time scales, but our ability to anticipate the existence and approximate location of a pouch (and associated sweet spot) exceeded prior expectations of many of the PIs. Recall that the sweet spot is the intersection of the wave trough axis and the wave critical line. This translates to an enhanced ability to anticipate the path along which genesis may occur, even though the exact timing of genesis remains uncertain due to the chaotic influence resulting from moist convection.

A practical outcome is the realization of a trackable feature in forecast models that can be treated much the same way as a tropical cyclone center, long before an identifiable organized storm exists! The predictability of the track of the sweet spot manifests qualitatively similar predictability as the track of a tropical cyclone. In particular, this suggests that ensembles of global and regional models should be effective in estimating a most likely path along which genesis can occur as well as providing the uncertainty in this path. While further research is necessary to quantify the predictability of "pouch tracks," we believe that the implications for improving tropical cyclone forecasts out to a week (the current goal of the National Hurricane Center), or perhaps even longer, using pouch tracking, are significant.

It became apparent also during PREDICT that the observations collected by the GV enhanced the subsequent skill of predicting the pouch track and pouch structure in operational and research models, and in several instances the data enhanced the skill of the genesis prediction itself. This was most evident in ex-Gaston, Karl, and Matthew, during which several missions were flown. An important question is "What aspect of the measurements was most important for enhancing predictive skill?" Another practical question is "How many flights are necessary to get cycling data assimilation systems on the right trajectory in model phase space?" Research will seek also to understand the relative contributions of convective-scale (Sippel and Zhang 2008, 2010; Nguyen et al. 2008; Shin and Smith 2008; Zhang and Sippel 2009) and meso-synoptic-scale uncertainties toward the limits of predictability of genesis.

A potentially significant link between the dynamics and thermodynamics of the nondeveloping Gaston case was suggested by the shallowing of Gaston's pouch over the 5-day observation period. A deteriorating pouch is hypothesized to enable the intrusion of dry air from outside with correspondingly low θ_e values. Such a link between dynamics and thermodynamics points to the usefulness of obtaining in situ data for characterizing the thermodynamic

and kinematic structure of candidate wave pouches. Further research is required for this case as well as the other developing and nondeveloping cases observed during PREDICT.

ACKNOWLEDGMENTS. This research was supported by the National Science Foundation Grants ATM-0733380, 0850709, 0851077, 0840651, and 1016095; NASA Grants NNH09AK561 and NNG09HG031; and a grant to MTM from NOAA's Hurricane Research Division. The scientists from the PREDICT team wish to express their gratitude to Stephen Nelson and Bradley Smull at NSF-ATM for providing helpful guidance through the planning stages of this experiment. The team expresses also their many thanks to Frank Marks Jr., of NOAA/AOML and Ramesh Kakar of NASA and the corresponding science teams of IFEX and GRIP for their enthusiastic collaboration and support. The authors thank the many members of the Earth Observing Laboratory of NCAR for their fantastic support of PREDICT. While there were too many people involved to list all of them, scientists Jose Meitin, Greg Stossmeister, Al Schanot, Al Cooper, Dave Rogers, Jeff Stith, Julie Haggerty, Cindy Twohy, and Darin Toohey were vital to the success of the project, as were operations managers Brigitte Baeuerle and Vidal Salazar. Pilots Henry Boynton, Scotty McClain, Steve Thompson, Ed Ringleman, and Lowell Genzlinger provided expert operation of the GV and were eager to work with the PIs to optimize the flight track given weather and air space restrictions. We wish to thank Gerald Thomsen and the German Weather Service for providing the ECMWF data. Numerous research scientists provided field support as well, including Tony Wimmers and Derrick Herndon (CIMSS) and Jason Dunion (NOAA/AOML/HRD). Numerous students and postdocs played a pivotal role in PREDICT, and they have summarized their experiences in a companion article (Evans et al. 2011). Finally, we wish to thank David Raymond and Carlos Lopez for their dedicated participation in the experiment and providing the team with valuable scientific input, debate, flight-planning support, and mission-scientist leadership.

REFERENCES

Anthes, R. A., and Coauthors, 2008: The COSMIC/FORMOSAT-3 mission: Early results. *Bull. Amer. Meteor. Soc.,* **89,** 313–333.

Bister, M., and K. A. Emanuel, 1997: The genesis of Hurricane Guillermo: TEXMEX analyses and a modeling study. *Mon. Wea. Rev.,* **125,** 2662–2682.

Davis, C. A., and L. F. Bosart, 2004: The TT problem: Forecasting the tropical transition of cyclones. *Bull. Amer. Meteor. Soc.,* **85,** 1657–1662.

DeMaria, M., J. A. Knaff, and B. H. Connell, 2001: A tropical cyclone genesis parameter for the tropical Atlantic. *Wea. Forecasting,* **16,** 219–233.

Dunion, J. P., 2011: Rewriting the climatology of the tropical North Atlantic and Caribbean Sea atmosphere. *J. Climate,* **24,** 893–908.

——, and C. S. Velden, 2004: The impact of the Saharan air layer on Atlantic tropical cyclone activity. *Bull. Amer. Meteor. Soc.,* **85,** 353–365.

——, and C. S. Marron, 2008: A reexamination of the Jordan mean tropical sounding based on awareness of the Saharan air layer: Results from 2002. *J. Climate,* **21,** 5242–5253.

Dunkerton, T. J., M. T. Montgomery, and Z. Wang, 2009: Tropical cyclogenesis in a tropical wave critical layer: Easterly waves. *Atmos. Chem. Phys.,* **9,** 5587–5646.

Dvorak, V., 1975: Tropical cyclone intensity analysis and forecasting from satellite imagery. *Mon. Wea. Rev.,* **103,** 420–430.

Elsberry, R. L., and P. A. Harr, 2008: Tropical Cyclone Structure (TCS08) field experiment science basis, observational platforms, and strategy. *Asia Pac. J. Atmos. Sci.,* **44,** 209–231.

Emanuel, K. A., 1994: *Atmospheric Convection*. Oxford University Press, 580 pp.

——, 2005: *Divine Wind: The History and Science of Hurricanes*. Oxford University Press, 285 pp.

Evan, A., J. Dunion, J. Foley, A. Heidinger, and C. Velden, 2006: New evidence for a relationship between Atlantic tropical cyclone activity and African dust outbreaks. *Geophys. Res. Lett.,* **33**, L19813, doi:10.1029/2006GL026408.

Evans, C., and Coauthors, 2012: The Pre-Depression Investigation of Cloud-Systems in the Tropics (PREDICT) field campaign: Perspectives of early career scientists. *Bull. Amer. Meteor. Soc.,* **93,** 173–187.

Fang, J., and F. Zhang, 2010: Initial development and genesis of Hurricane Dolly (2008). *J. Atmos. Sci.,* **67,** 655–672.

——, and ——, 2011: Evolution of multiscale vortices in the development of Hurricane Dolly (2008). *J. Atmos. Sci.,* **68,** 103–122.

Frank, N. L., 1970: Atlantic tropical systems of 1969. *Mon. Wea. Rev.,* **98,** 307–314.

Garrison, J. L., and Coauthors, 2007: Development and testing of the GISMOS instrument. *Proc. IEEE Int. Geoscience and Remote Sensing Symp.,* Barcelona, Spain, IEEE, 5105–5108.

Gray, W. M., 1968: Global view of the origin of tropical disturbances and storms. *Mon. Wea. Rev.,* **96,** 669–700.

——, 1998: The formation of tropical cyclones. *Meteor. Atmos. Phys.,* **67,** 37–69.

Halverson, J., M. Black, and S. Braun, 2007: NASA's Tropical Cloud Systems and Processes Experiment: Investigating tropical cyclogenesis and hurricane intensity change. *Bull. Amer. Meteor. Soc.,* **88,** 867–882.

Hawkins, J., and C. Velden, 2011: Supporting meteorological field experiment missions and postmission analysis with satellite digital data and products. *Bull. Amer. Meteor. Soc.,* **92,** 1009–1022.

Herman, R. L., and A. J. Heymsfield, 2003: Aircraft icing at low temperatures in Tropical Storm Chantal (2003). *Geophys. Res. Lett.,* **30,** 1955, doi:10.1029/2003GL017746.

Houze, R. A., W.-C. Lee, and M. M. Bell, 2009: Convective contribution to the genesis of Hurricane Ophelia (2005), *Mon. Wea. Rev.,* **137,** 2778–2800.

James, R. P., and P. M. Markowski, 2010: A numerical investigation of the effects of dry air aloft on deep convection. *Mon. Wea. Rev.,* **138,** 140–161.

Jones, T. A., D. J. Cecil, and J. Dunion, 2007: The environmental and inner-core conditions governing the intensity of Hurricane Erin (2007). *Wea. Forecasting,* **22,** 708–725.

McBride, J. L., and R. Zehr, 1981: Observational analysis of tropical cyclone formation. Part II: Comparison of non-developing versus developing systems. *J. Atmos. Sci.,* **38,** 1132–1151.

McWilliams, J., 1984: The emergence of isolated coherent vortices in turbulent flow. *J. Fluid Mech.,* **146,** 21–43.

Meng, Z., and F. Zhang, 2008a: Test of an ensemble Kalman filter for mesoscale and regional-scale data assimilation. Part III: Comparison with 3DVAR in a real-data case study. *Mon. Wea. Rev.,* **136,** 522–540.

——, and ——, 2008b: Test of an ensemble Kalman filter for mesoscale and regional-scale data assimilation. Part IV: Comparison with 3DVAR in a month-long experiment. *Mon. Wea. Rev.,* **136,** 3671–3682.

Montgomery, M. T., and R. K. Smith, 2010: Tropical cyclone formation: Theory and idealized modeling. *Proc. Seventh Int. Workshop on Tropical Cyclones,* La Reunion, France, CSIRO. [Available online at www.cawcr.gov.au/projects/iwtc/documentation.php.]

——, M. E. Nicholls, T. A. Cram, and A. B. Saunders, 2006: A vortical hot tower route to tropical cyclogenesis. *J. Atmos. Sci.,* **63,** 355–386.

——, L. L. Lussier III, R. W. Moore, and Z. Wang, 2010a: The genesis of Typhoon Nuri as observed during the Tropical Cyclone Structure 2008 (TCS-08) field experiment—Part 1: The role of the easterly wave critical layer. *Atmos. Chem. Phys.,* **10,** 9879–9900.

——, Z. Wang, and T. J. Dunkerton, 2010b: Coarse, intermediate and high resolution numerical simulations of the transition of a tropical wave critical layer to a tropical storm. *Atmos. Chem. Phys.,* **10,** 10803–10827.

National Hurricane Center, 2010: Glossary of NHC terms. [Available online at www.nhc.noaa.gov/aboutgloss.shtml.]

Nguyen, V. S., R. K. Smith, and M. T. Montgomery, 2008: Tropical-cyclone intensification and predictability in three dimensions. *Quart. J. Roy. Meteor. Soc.,* **134,** 563–582.

Raymond, D. J., and C. López-Carillo, 2011: The vorticity budget of developing Typhoon Nuri (2008). *Atmos. Chem. Phys.,* **11,** 147–163.

——, ——, and L. López-Cavazos, 1998: Case-studies of developing east Pacific easterly waves. *Quart. J. Roy. Meteor. Soc.,* **124,** 2005–2034.

Reale, O., W. K. Lau, K.-M. Kim, and E. Brin, 2009: Atlantic tropical cyclogenetic processes during SOP-3 NAMMA in the GEOS-5 global data assimilation and forecast system. *J. Atmos. Sci.,* **66,** 3563–3578.

Reasor, P. D., M. T. Montgomery, and L. F. Bosart, 2005: Mesoscale observations of the genesis of Hurricane Dolly (1996). *J. Atmos. Sci.,* **62,** 3151–3171.

Sadler, J. C., 1976: A role of the tropical upper tropospheric trough in early season typhoon development. *Mon. Wea. Rev.,* **104,** 1266–1278.

Shin, S., and R. K. Smith, 2008: Tropical-cyclone intensification and predictability in a minimal three-dimensional model. *Quart. J. Roy. Meteor. Soc.,* **134,** 1661–1671.

Shu, S., and L. Wu, 2009: Analysis of the influence of the Saharan air layer on tropical cyclone intensity using AIRS/*Aqua* data. *Geophys. Res. Lett.,* **36,** L09809, doi:10.1029/2009GL037634.

Sippel, J. A., and F. Zhang, 2008: Probabilistic evaluation of the dynamics and predictability of tropical cyclogenesis. *J. Atmos. Sci.,* **65,** 3440–3459.

——, and ——, 2010: Factors affecting the predictability of Hurricane Humberto (2007). *J. Atmos. Sci.,* **67,** 1759–1778.

Skamarock, W. C., J. B. Klemp, J. Dudhia, D. O. Gill, D. M. Barker, W. Wang, and J. G. Powers, 2005: A description of the Advanced Research WRF version 2. NCAR Tech. Note TN-468+STR, 88 pp.

Sun, D., W. K. M. Lau, M. Kafatos, Z. Boybeyi, G. Leptoukh, C. Yang, and R. Yang, 2009: Numerical simulations of the impacts of the Saharan air layer on Atlantic tropical cyclone development. *J. Climate,* **22,** 6230–6250.

Torn, R. D., 2010: Performance of a mesoscale ensemble Kalman filter (EnKF) during the NOAA

high-resolution hurricane test. *Mon. Wea. Rev.,* **138,** 4375–4392.

——, and G. J. Hakim, 2008: Ensemble-based sensitivity analysis. *Mon. Wea. Rev.,* **136,** 663–677.

Wang, Z., M. T. Montgomery, and T. J. Dunkerton, 2009: A dynamically-based method for forecasting tropical cyclogenesis location in the Atlantic sector using global model products. *Geophys. Res. Lett*., **36**, L03801, doi:10.1029/2008GL035586.

——, ——, and ——, 2010a: Genesis of pre-Hurricane Felix (2007). Part I: The role of the wave critical layer. *J. Atmos. Sci.,* **67,** 1711–1729.

——, ——, and ——, 2010b: Genesis of pre-Hurricane Felix (2007). Part II: Warm core formation, precipitation evolution and predictability. *J. Atmos. Sci.,* **67,** 1730–1744.

——, ——, and C. Fritz, 2011: A first look at the structure of the wave pouch during the 2009 PREDICT-GRIP "dry run" over the Atlantic. *Mon. Wea. Rev.,* in press.

Weiss, J., 1991: The dynamics of enstrophy transfer in two-dimensional hydrodynamics. *Physica D,* **48**, 273–294.

Wimmers, A. J., and C. S. Velden, 2007: MIMIC: A new approach to visualizing satellite microwave imagery of tropical cyclones. *Bull. Amer. Meteor. Soc.,* **88,** 1187–1196.

——, and ——, 2011: Seamless advective blending of total precipitable water retrievals from polar-orbiting satellites. *J. Appl. Meteor. Climatol.,* **50,** 1024–1036.

Wu, L., 2007: Impact of Saharan air layer on hurricane peak intensity. *Geophys. Res. Lett.,* **34**, L09802, doi:10.1029/2007GL029564.

Xie, F., J. S. Haase, and S. Syndergaard, 2008: Profiling the atmosphere using the airborne GPS radio occultation technique: A sensitivity study. *Trans. IEEE Geosci. Remote Sens.,* **46,** 3424–3435.

Zhang, F., and J. A. Sippel, 2009: Effects of moist convection on hurricane predictability. *J. Atmos. Sci.,* **66,** 1944–1961.

——, Y. Weng, J. A. Sippel, Z. Meng, and C. H. Bishop, 2009: Cloud-resolving hurricane initialization and prediction through assimilation of Doppler radar observations with an ensemble Kalman filter. *Mon. Wea. Rev.,* **137,** 2105–2125.

Zipser, E. J., and Coauthors, 2009: The Saharan air layer and the fate of African easterly waves—NASA's AMMA field study of tropical cyclogenesis. *Bull. Amer. Meteor. Soc.,* **90,** 1137–1156.